Published in final edited form as:

Langmuir. 2021 April 20; 37(15): 4611–4621. doi:10.1021/acs.langmuir.1c00290.

Tuning cationic micelle properties with antioxidant additive: a molecular perspective

Vinod Kumar[1,#], **Geetha M Sai**[2,#], **Rajni Verma**[3], **Katie R. Mitchell-Koch**[3], **Debes Ray**[4], **Vinod Kumar Aswal**[4], **Prachi Thareja**[2], **Ketan Kuperkar**[1], **Pratap Bahadur**[5]

[1]Department of Chemistry, Sardar Vallabhbhai National Institute of Technology (SVNIT), Surat-395 007, Gujarat, INDIA.

[2]Department of Chemical Engineering, Indian Institute of Technology (IIT), Gandhinagar 382 355, Gujarat, INDIA

[3]Department of Chemistry, Wichita State University (WSU), Wichita, Kansas 67260-0051, USA.

[4]Solid State Physics Division, Bhabha Atomic Research Centre (BARC), Mumbai 400 085, INDIA.

[5]Department of Chemistry, Veer Narmad South Gujarat University (VNSGU), Udhana-Magdalla road, Surat 395 007, Gujarat, INDIA.

Abstract

In this work, we characterize the micellization and morphology transition induced in aqueous solution of cetyltrimethylammonium bromide (CTAB) by the addition of an antioxidant propyl gallate (PG) using tensiometry, rheology and small-angle neutron scattering (SANS) techniques unified with molecular dynamics (MD) simulation approach. The adsorption of CTAB at air-water interface in the presence of varying [PG] revealed a progressive decrease in the critical micelle concentration (CMC) while the changes in different interfacial parameters ascribed to enhance the hydrophobicity induced by PG in the CTAB micellar system. The dynamic rheology behavior indicated an increase in the flow viscosity (η) as a function of [PG]. Moreover, the rheological components (storage modulus, *G'* and loss modulus, *G"*) depicted the viscoelastic features. SANS measurements depicted the existence of ellipsoidal micelles with varying size and aggregation number (N_{agg}) as a function of [PG] and temperature. Computational simulation performed using density functional theory (DFT) calculations and molecular dynamics (MD) probed an insight into the atomic information of the examined system. Here, the molecular electrostatic potential (MEP) analysis depicted a close proximity of CTAB i.e., emphasized favorable interactions between the quaternary nitrogen of CTAB and hydroxyl group of PG monomer which is further validated from two-dimensional nuclear Overhauser enhancement spectroscopy (2D-NOESY) which inferred the penetration of PG inside CTAB micelles. In addition, various dynamic properties *viz.,* the radial distribution function (RDF), the radius of gyration (R_g) and solvent-accessible surface area (SASA) showed the significant microstructural evolution of the ellipsoidal micelles in the examined CTAB-PG system where the changes in the micellar morphology with more elongated

Corresponding Author: Dr. Ketan Kuperkar, ketankuperkar@gmail.com.

[#]Equal contribution in this work

CONFLICT OF INTEREST

The authors declare no conflict of interest.

hydrophobic chain, and increased R_g and SASA values inferred the notable intercalation of PG in the CTAB micelles.

Graphical Abstract

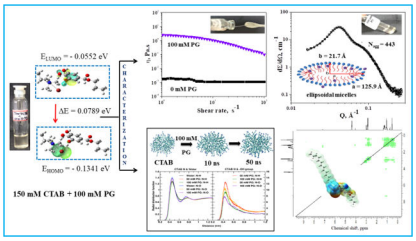

Schematic illustration depicting the self-association and aggregation conduct in aqueous viscoelastic ellipsoidal CTAB-PG system substantiated with molecular dynamics approach.

Keywords

Surfactant micelles; antioxidant; solution rheology; radial distribution function (RDF); solvent-accessible surface area (SASA); molecular electrostatic potential (MEP)

INTRODUCTION

Cationic surfactants exhibit a wide range of self-assembled geometries ranging from spherical micelles to short-rods (ellipsoidal) or long-cylinders to entangled worm-like micelles, vesicles and liquid crystalline edifices giving an account to their concentration in aqueous solution.[1–3] Studies have reported that these nanoscale morphologies can be fine-tuned by altering the solution environment in the presence of various organic/inorganic additives (anionic hydrotropes, short chain surfactants, salts, etc.) manipulating the temperature, pH, ionic strength, etc.[4–10] Such alteration in micellar characteristics impart them the ability to serve as *smart* materials with excellent potential for rheology control, enhanced oil recovery, delivery of hydrophobic bioactive molecules, etc.[11–15] However, to achieve the microstructures of higher order such as worm-like micelles, vesicles, or liquid crystals, the truthful selection of additives is very crucial.

Amongst this, the highly viscous or viscoelastic systems in the cationic surfactants with rod-like or worm-like micellar assemblies have drawn significant research interest.[16] Khatory *et al*. reported worm-like micelle formation in cetyltrimethylammonium bromide (CTAB) in the presence of potassium bromide (KBr) with the linear and non-linear viscoelasticity.[17] There have been several reports on using inorganic anions like nitrate, perchlorate and organic anions like salicylate, *p*-toluene sulphonate, etc. depicting the micellar transition from spherical micelle to worm-like micelles.[10, 18–21]

In addition to this, the literature studies have reported the induced micellar transitions by solubilizing several drugs as effective additives. Amid the varied class of drugs, a specific focus on antioxidants (gallates) has been put forth giving an account on its effective degree of binding with ionic surfactants thereby offering an insight into the operative

mixed formulations for biomedical applications.[22–25] In particular, propyl gallate (PG) is widely studied due to its moderate hydrophilic nature and slow oxidation kinetics.[26] Anna *et al.* studied the co-adsorption of CTAB and PG on the hydrophilic silica surface and suggested that the main driving force for adsorption of PG is its interaction with hydrophobic moieties of preliminary CTAB aggregates.[26] Heins *et al.* have presented the solubilization and location of PG in the micellar phase of CTAB, sodium dodecyl sulphate (SDS) and polyoxyethylene-20-cetyl ether (Brij 58) where strong effects of sphere-to-rod micellar transition was observed in case of CTAB with the increasing depth of PG intercalation following the order: SDS < Brij 58 < CTAB.[24, 27] Szymula *et al.* investigated the electrochemical oxidation of PG to be an irreversible and strongly pH dependent process using cyclic voltammetry where it was found that the addition of CTAB solutions influenced the oxidation potential and the peak current.[28] Also, the theoretical investigations have offered a better understanding and served a predictive tool in depicting the surfactant behavior in presence of additives. In the past decade, molecular dynamics (MD) simulation studies have presented the analysis and mechanism of micellar aggregation and structural transitions at atomistic level.[29–32] Sangwai *et al.* carried out MD simulations on cetyltrimethylammonium chloride (CTAC) molecule with effects of sodium salicylate and sodium chloride.[33] Yuan *et al.* preformed MD simulation to investigate the structural and dynamic properties of CTAB monolayer formed at the air-water interface.[34] Velinova *et al.* inferred the micellar transition of pentaethylene glycol monododecyl ether ($C_{12}E_5$) from spherical to rod-like shape by MD simulation.[35] Chen *et al.* offered a detailed insight into the dynamic properties at fixed surfactant numbers by considering different ratios of CTAB and sodium octyl sulfate aqueous mixtures.[36] However, investigation focussing on the quantitative effects of PG into CTAB is still very scarcely presented.

Hence, we present a systematic study underlying the effect of an antioxidant (propyl gallate, PG) in CTAB micelles using experimental and theoretical approach. We have used PG with an intention to achieve this aim. With the structural hydrophobic and hydrophilic regions, PG serves as a perfect model molecule to probe the influence as an additive on the microstructure of CTAB micelles. Here, physical methods viz., tensiometry and rheometry offer an insight into the micellization conduct in CTAB yielding critical micelle concentration (CMC) and adsorption parameters at air-water interface along with the rheological behavior intending to influence the solution flow viscosity (η) as a function of [PG]. The micelle size/shape and aggregation (N_{agg}) are estimated from the small-angle neutron scattering (SANS) data analysis. Computational simulations provide an utmost account through the density functional theory (DFT) calculations in terms of the energy gap (ΔE), the total energy (TE), and electrostatic potential (MEP) along with the groping of the radial distribution functions (RDF), the radius of gyration (R_g) and solvent-accessible surface area (SASA) from Molecular Dynamics which will probe the microstructural evolution involved in the examined CTAB-PG system. In addition, the intercalated solubilization site of PG in CTAB micelle is further validated from two-dimensional nuclear Overhauser enhancement spectroscopy (2D-NOESY).

EXPERIMENTAL

Materials

The cationic surfactant: cetyltrimethylammonium bromide (CTAB) and antioxidant: propyl gallate (PG) were purchased from TCI Chemicals, Japan and used as received. All the sample solutions were prepared by dissolving precisely weighed amounts of the solute in necessary volume of de-ionized double distilled water. Deuterium oxide (D_2O, 99.9 % D atom) solvent was used to prepare sample solutions for scattering and spectral experiments.

Methods

Tensiometry—Surface tension (ST; γ) measurements the air-water interface were performed following the "du Noüy" ring method using Kruss tensiometer (Kruss K9, Germany) at ~ 30 °C. The platinum ring was thoroughly washed with acetone followed by de-ionized double distilled water after each measurement. The critical micelle concentrations (CMCs) were observed as a sharp break in the intersection points in γ against the logarithm of surfactant concentration curves. The uncertainty in ST measurements was ± 0.1 mN/m.

Various surface parameters like effective surface tension reduction at CMC (π_{CMC}) and maximum surface excess concentration (Γ_{max}) were calculated using the classical Gibbs adsorption equation which offers a solid foundation for the experimental data analysis on the ST and the surface concentration of surfactants.

$$\Gamma_{\max} = -\frac{1}{2.303nRT}\left[\frac{d\gamma}{dlogC}\right] \quad (1)$$

where R = 8.314 $Jmol^{-1}K^{-1}$ (universal gas constant), T is the absolute temperature (303.15 K), C is surfactant concentration (mol/L), N_A is the Avogadro number, and n is dissociation number of the surfactant molecules formed in the solution and is taken as 2 for CTAB surfactant.[37–39]

Rheology—The rheological properties were measured by stress-controlled Anton Paar modular compact rheometer (MCR 302). Parallel plate geometry of 50 mm diameter with a measuring gap of 0.5 mm was used for the oscillatory and shear rheology measurements. Shear rheology of CTAB-PG solutions was conducted from 1–100 s^{-1} at 30 °C with varying [PG]. The viscosity of 150 mM CTAB in the presence of PG was measured at a constant shear rate of 1 s^{-1} from 30 °C to 70 °C in both forward and backward temperature ramps. The viscosity of 100 mM and 150 mM PG solution was measured at 30 °C and 50 °C to study the effect of the temperature. The thermo-responsive behavior of 150 mM CTAB and 150 mM PG solution was studied by measuring the viscosity by alternatively applying 30 °C and 50 °C for 10 minutes up to 2 cycles by shearing the samples at a constant shear rate of 1 s^{-1}. Here, small amplitude oscillatory frequency sweep measurements were performed from 100 to 0.1 rad/s of angular frequency (ω) at an oscillatory strain of 0.5 %. These measurements are ensured to be in the linear viscoelastic regime. A solvent trap filled with water was used to minimize the evaporative losses.

Small-angle neutron scattering (SANS)—The scattering experiments were performed on SANS diffractometer at Dhruva reactor-BARC, India which uses a velocity selector-monochromatized beam of mean wavelength (λ) of 5.2 Å with resolution (Δλ/λ) of ~ 10 %. The angular distribution of the scattered neutrons was recorded using a linear 1 m-long He^3 one-dimensional position-sensitive detector (PSD). Here, the data are expressed as absolute intensity versus the accessible scattering wave vector ($Q = 4\pi\sin\theta/\lambda$, where 2θ is the scattering angle) in the range of 0.017–0.35 $Å^{-1}$. The PSD permits simultaneous data recording over the full Q-range. The scattering spectra were corrected on an absolute scale. The tested solutions were placed in a 0.5 cm quartz cell cuvette with Teflon stoppers and the scattering measurements were recorded at required temperature. All the measured scattering distributions were corrected for the background and solvent contributions which were normalized to the cross-sectional unit using standard procedures.[40–41]

The coherent differential scattering cross-section, dΣ/dΩ per unit volume of solution for interacting micelles is given by[10, 42]:

$$\frac{d\sum}{d\Omega} = n_m V^2(\rho_m - \rho_s)^2\left\{\langle F^2(Q)\rangle + \langle F(Q)\rangle^2[S(Q) - 1]\right\} + B \quad (2)$$

where n_m denotes the number density of the micelles, V is the micelle volume, ρ_m and ρ_s are the scattering length densities of the micelle and the solvent, respectively. F(Q) is the single particle (intraparticle) form factor, S(Q) is the interparticle structure factor, and B is a constant term that represents the incoherent scattering background, which is mainly due to hydrogen in the sample.

The single particle form factor has been calculated by treating the micelles as prolate ellipsoids.

$$\langle F^2(Q)\rangle = \int_0^1 [F(Q,\mu)]^2 d\mu \quad (3)$$

$$\langle F(Q)\rangle^2 = [\int_0^1 F(Q,\mu)d\mu]^2 \quad (4)$$

$$F(Q,\mu) = \frac{3(\,sinx - xcosx\,)}{x^3} \quad (5)$$

$$x = Q\,[a^2\mu^2 + b^2(1-\mu^2)]^{1/2} \quad (6)$$

where a and b are the semi-major and semi-minor axes of an ellipsoidal micelle, respectively, and μ is the cosine of the angle between the directions of a and the wave vector transfer Q.[10]

The interparticle structure factor S(Q) specifies the correlation between the centres of different micelles and it is the Fourier transform of the radial distribution function g(r)

for the mass centres of the micelle. Unlike the calculation of F(Q), it is quite complicated to calculate S(Q) for any shapes other than spherical. This is because S(Q) depends on the shape as well as on the orientation of the particles. *To simplify this, prolate ellipsoidal micelles are assumed to be equivalent to spherical micelles*. For the ellipsoid micellar model, the expression derived by Hayter and Penfold was used.[43] The aggregation number (N_{agg}) is defined as the total number of the (surfactant monomer and additive) molecules that associate together to form a micelle, was evaluated from the relation: $N_{agg} = 4\pi ab^2/3v$, where v is the volume of surfactant monomer, estimated here using the Tanford formula, which support the idea of micellar growth/transition.[44] Thus, the micellar dimension, structure factor parameters and N_{agg} were determined from the scattering analysis.

Two dimensional-Nuclear Overhauser Enhancement Spectroscopy (2D-NOESY)—The 2D-NOESY was recorded using a Bruker AVANCE-II 400 MHz spectrometer. The mixing times and the delay times for experiments have been assessed by the spin-lattice relaxation times (T_1 values) of the surfactant determined in separate experiments. Here, the acquisition delay of ≈ 3×T_1 and a mixing time of ≈ 1×T_1 have been used to obtain the 2D-NOESY spectra. The required set of experiment was completed in phase-sensitive mode, with and without the saturation of the water resonance at ~ 4.70 ppm. The data have been zero-filled twice in dimension 1 and multiplied by a squared sine function in both dimensions before 2DFT.[43, 45]

Computational simulation approach—The molecular structures of pure ingredients: CTAB and PG were optimized using the density functional theory (DFT)/B3LYP with basis set 3–21G method of Gauss View 5.0.9 package with Gaussian 09W calculation window. Various optimized descriptors such as the highest occupied molecular orbital (HOMO), lowest unoccupied molecular orbital (LUMO), the energy band gap (ΔE = $E_{LUMO} - E_{HOMO}$) and the 3D-Molecular Electrostatic Potential (3D-MEP) surface data were evaluated for the examined system.[46–47]

In addition, the molecular dynamics (MD) of 150 mM CTAB micelles were performed in the aqueous solution containing 0 mM, 50 mM, and 100 mM PG using Gromacs software package.[48] A spherical aggregate of 100 CTAB monomers was constructed using Packmol software.[49] The spherical CTAB micelle was centered in a ~11 nm cubic box of aqueous solution to perform MD simulation at 30 °C. PG molecules were randomly placed in the simulation box. GROMOS96 54a7[50] force field for CTAB and PG from Automated Topology Builder was adopted.[51–52] The system was first energy minimized for 10000 steps using the steepest descent algorithm to remove bad clashes between the atoms. After energy minimization, all the atoms were given an initial velocity obtained from a Maxwellian distribution. A time step of 2 fs was used to integrate the equations of motion for all the simulations. First, the system was equilibrated for 50 ps by applying position restraints to the heavy atoms of the CTAB molecules for solvent relaxation in the simulation box. Then the position restraints were removed, and the system was gradually heated from 0 °C to 30 °C during 200 ps of the simulation. After equilibration, a production run of 50 ns was performed for the CTAB micelle simulations in aqueous solution of 0 mM, 50 mM and 100

mM PG. The simulation data were used to understand the solvation and structural properties of CTAB micelle with increasing concentrations of PG (Table 1).

RESULTS AND DISCUSSION

Air-water interfacial conduct

Figure 1 depicts the surface tension (ST, γ) versus surfactant concentration (*in logarithm scale*) plot for CTAB at different concentrations of PG at 30 °C. Here, at low concentrations, CTAB molecules tend to adsorb at the air-water interface until its saturation at the surface resulting in a sharp break point generally referred as critical micelle concentration (CMC); above which the ST is almost constant. Here, the measured CMC value of CTAB in water (i.e., in absence of PG) is in good agreement with the reported value.[18, 53] However, with increasing concentration of PG, the CMC as well as the γ decreases, which shows that PG promotes quicker micellization in CTAB. Such behavior could be attributed to the induced hydrophobicity of PG in CTAB.

Based on the Figure 1, various interfacial parameters of CTAB as a function of [PG] in aqueous solution are evaluated (Table 2). The Γ_{max} value of CTAB decreases with an increase in [PG] which show that the saturation of the interface has been reached, tending the CTAB molecules to start solubilizing into the bulk solution. These findings are in good agreement with the reported studies.[54] It was also observed that π_{CMC} increases with the increasing [PG] thereby indicating enhanced efficiency of PG to reduce the γ as compared to pure CTAB in water.

Rheology demeanor

Figure 2a depicts the flow viscosity (η) trend in ~ 150 mM CTAB with applied shear rate in the presence of varying [PG] at 30 °C. The CTAB solutions with 0 to 50 mM of [PG] show an independent η with an increased shear rate, which is a typical characteristic of the Newtonian behavior. Here, as the [PG] increases, the η increases dramatically giving a hint of plausible morphology change in CTAB micelles in the presence of antioxidants.[24] i.e., the solution with 100 mM PG show higher η and a shear-thinning behavior in the entire range of shear from 1 to 100 s^{-1}, which demonstrates the formation of higher micellar geometry, probably the elongated ellipsoidal or rod-/worm-like micelles in the examined systems. These findings are in agreement with the reported study.[10, 55] The value of η decreases further with increase in [PG] (150 mM). This depicts a reduction in the micellar size or due to apparent branching that is caused by micellar dynamic peristalsis.[56] The solution exhibits Newtonian behavior again up to 50 s^{-1} and starts displaying shear thinning behavior with further increase in shear rate. Such a trend is attributed to the favorable hydrophobic interaction between PG and CTAB that leads to a compact packing due to increase in the ratio of CTAB molecules at the micellar surface. Figure 2b depicts the temperature dependence on η and offers an insight into the versatility of CTAB micelles when subjected to temperature change. It was observed that η of the examined solutions decreases with increase in the temperature as the length of the micelles of high geometry order decreases.[57] In the forward temperature ramp, as the temperature is raised, the η starts decreasing till 60 °C and later increases slightly, while in the backward temperature

ramp, the η show a continuous increase with decreasing temperature. Such clear distinctive behavior is illustrated in the insight image of Figure 2b.

The Figure 2c presents the rheological behavior in 150 mM CTAB-150 mM PG that can be easily controlled by adjusting the ambient temperature via a preset procedure. Initially, when the sample is at 30°C, η remains constant at 10 Pa.s and as the temperature increases from 30 °C to 50 °C at a rate of 2 °C/min, η gradually decreases from 10 Pa.s to 0.9 Pa.s. During cooling down the sample to 30 °C, the η returns to its original value of 10 Pa.s showing its thermo-responsive behavior. After two heating/cooling cycles, the η can still regain its original state. The typical behavior of η is due to the changes in micellar structure.[58] Here, the sample solution of 150 mM CTAB + 150 mM PG appears like a soft-gel that flows under small perturbations which is been further supported by the measurements of of G' and G'' as a function of small amplitude oscillatory frequency sweep (ω) (Figure 2d). Here, both the solutions show $G'' > G'$ in the low ω region depicting liquid-like behavior while the same exhibited solid-like ($G' > G''$) behavior in the high ω region. This typical viscoelastic behavior of micellar solutions infer the presence of higher range of micellar geometry than the spherical micelles. At 100 mM PG, the cross-over of G' and G'' occurred at a lower ω (~ 7.19 rad/s), i.e., high relaxation time. When the PG concentration increases to 150 mM, G' and G'' decrease, and the cross-over shifts to higher ω from (~ 78.79 rad/s) i.e., low relaxation time. Studies have reported such trend in the relaxation processes due to the plausible micellar transition into a less rigid network geometry with an increase in additive concentration.[59–60]

Scattering behavior

Small-angle neutron scattering (SANS) profile offered a quantitative evaluation to our study depicting the change in the micellar dimension/shape in CTAB under the influence of [PG] and temperature (Figure 3).

The evolution of SANS spectra for 150 mM CTAB solution at 30 °C revealed an increase in the normalized peak intensity in the presence of varying [PG] thereby inferring an increase in the micellar size (Figure 3a). The correlation peaks ($Q = 2\pi/d$) are allied with the distance between CTAB and PG that shifts towards the low Q region. This clearly indicates a decrease in the range of electrostatic interaction in the examined system as a function of [PG]. The results also show the influence of temperature, where the normalized peak intensity decrease thereby indicating a decrease in the size of micelles (Figures 3b–d). Giving an account to the reported work, we anticipated that 150 mM CTAB solution system in absence of PG when subjected to temperature change results into the formation of shorter micelles and hence the data were not measured to make suitable comparison.[61]

The fitting analysis show that the size of CTAB micelles increases with increasing concentration of PG (Table 3). Here, the N_{agg} as well as semi-major axis (a) increase in 150 mM CTAB for 10, 25, 50 and 100 mM PG due to the formation of large micelles while the decrease in the micelle size is noticed for 150 mM CTAB in presence of 150 mM PG that attribute to the formation of small micellar aggregates due to the apparent branching or less rigid network geometry.[56] Such findings are well in agreement with the noted rheological behavior for the examined system. Also, the values of N_{agg} and semi-major axis (a) decrease

with increasing temperature. This could be due to the increased dissociation of counter-ions at higher temperature, resulting in stronger repulsion among the charged head groups. As a result, the effective area of the head group per surfactant molecule increases and indicates a reduction in the packing parameter thereby favouring smaller micelles. Such performance is further supported by spectral study and furthermore validated employing computational simulation approach.

Spectral investigation

Figure 4 presents the recorded 2D-NOESY spectrum for the examined (150 mM CTAB and 25 mM PG) system which showed intense correlation peaks between the carbon terminal-chain (H_γ to H_ω) protons in the region of ~ 0.5 to ~ 1.7 ppm. In addition, strong correlation peak between N-CH_3 protons of CTAB and terminal-chain protons (H_a and H_b) of PG was noticed around ~ 2.9 ppm while the spectrum displayed weak cross-peaks between H_c proton of PG and H_α and H_β protons of CTAB at ~ 4.1 ppm. In addition, correlation peak between aromatic ring protons of PG and terminal-chain protons of CTAB was noticed around ~ 7.3 ppm. Thus, the spectral findings inferred that the PG molecule intercalate in the CTAB micelle thereby plausibly giving a hint of favorable interaction between CTAB and PG. This depiction goes well with the reported work.[62–63]

Theoretical endorsement

Figure 5a offer an acumen into the dependence on the orbital energy difference in the examined system. It can be clearly seen that the electronic density in the HOMO and LUMO of each CTAB-PG system is quite uniform, which is due to the π-electron cloud density of these systems. The ΔE value of CTAB-PG (0.0789 eV) system is lower than its pure ingredients: CTAB (0.1884 eV) and PG (0.1719 eV) respectively which suggests that the PG has a strong ability to undergo effective interaction with CTAB. The CTAB-PG complex is 0.05 eV lower in energy than the individual components thereby indicating favorable interactions and although it should be noted that dispersion forces and electron correlation are not accounted for these calculations.[64–65] Studies have also explained the importance of dipole moment (μ) as the measure of the interaction between the molecules. However, it depends on the type and nature of molecules considered. Similar to the reported results, our findings showed increased value of μ for the CTAB-PG aggregate relative to the individual components. This indicates favorable accumulation of PG onto the surface of CTAB, which in turn contributes to the effective interaction between them i.e., μ of CTAB-PG (~ 13.21 D) is greater than CTAB (~ 12.03 D) and PG (~ 3.41 D) respectively which indicate the stronger interaction ability of CTAB with PG.

In addition to this, the 3D-molecular electrostatic potential (3D-MEP) descriptor has shown the charge distribution of corresponding atoms which evidently predicted the coordinating electrophilic centers of PG and nucleophilic sites of CTAB head group considering the electron charge density distribution around nitrogen and neighboring carbon atoms of PG (Figure 5b). The red (*nucleophilic centers*), blue (*electrophilic sites*), and green regions indicate the most negative, most positive, and zero MEP regions, respectively. Here, the color spectrum of MEP is mapped to all other values by linear interpolation within the range: − 7.848 e^{-2} to + 7.848 e^{-2} for PG, − 8.871 e^{-2} to + 8.871 e^{-2} for CTAB and −9.644

e^{-2} to + 9.644 e^{-2} for CTAB-PG in the linear interpolation range that show more close proximity of the CTAB with PG inferring more favorable interactions between the nitrogen atom of CTAB and hydroxyl group of PG which is already been predicted by 2D-NOESY.

The molecular dynamics (MD) offered a further understanding into the experimental observation for CTAB micelles in the absence and presence of PG. The behavior of CTAB micelles is entirely affected by aqueous solution around it. The solvation of CTAB micelle was first assessed using radial distribution function (RDF) that predicted the average packing of solvent molecules around the CTAB micelle. RDF was calculated from the nitrogen (N) atom of CTAB molecule to oxygen (O) and hydrogen (H) atoms of water and hydroxyl (−OH) group of PG. The probability of solvent density around the CTAB-N in varying [PG] solution is also shown in Figure 6. During the simulations, the first and second hydration shells are located at ~ 0.45 nm and ~ 0.76 nm, respectively for water molecules. In the first solvation shell, the average cumulative number of water molecules around the micelle is ~7. In the presence of PG, RDF values of hydration shell indicate a similar distribution of water molecules with slightly lower peak intensity around the trimethylammonium group of CTAB micelle. In PG solution environment, the first solvation shell is located at ~ 0.42 nm and has one PG molecule coordinated with CTAB monomer. At 100 mM PG concentration, lower peak intensities are observed which could be explained by the occurrence of PG aggregates in the simulation.

The CTAB micellar aggregate remains stable throughout the simulations in 0 mM, 50 mM, and 100 mM PG solution. Figure 7 illustrates the dynamic behavior of CTAB micellar aggregation. It is seen that the bromide ion remains at an average distance of ~ 0.5 nm during the simulations as observed earlier in the reported simulation studies.[32, 66]

The distance between two N atoms in the CTAB micelle was studied using the RDF. Neighboring head groups are located with a most probable distance of 0.83 nm, which is consistent with earlier observation of N-N distance in the simulation of aqueous CTAB micelle by Cata *et al.*[66] The beginning to end distances of the hydrophobic tail shows an average of ~ 1.58 ± 0.2 nm in 0 mM and 50 mM PG solution, and ~ 1.62 ± 0.2 nm in 100 mM PG solution respectively. The CTAB micelle immediately changes its morphology from spherical to the ellipsoidal structure during the simulations. In addition, we have also assessed the radius of gyration (R_g) of the micelle which measures the compactness of the structure.[32] The starting structure of spherical CTAB micelle has R_g of ~ 2.07 nm. During the simulations, CTAB micelles go through the solvent-induced changes in the shape. After 30 ns of equilibration time, CTAB micelles have an average R_g of ~ 2.09 ± 0.41 nm in 0 mM PG solution. R_g values increased with a growing concentration of PG to ~ 2.14 ± 0.58 nm and ~ 2.16 ± 0.41 nm in 50 mM and 100 mM aqueous solution respectively.

Furthermore, we have calculated the solvent-accessible surface area (SASA) to understand the hydrophobic and hydrophilic properties of the micellar aggregates in aqueous solution. Figure 8 (i–iii) show the SASA of CTAB micelles and the snapshot of CTAB micelles using last frame of 50 ns simulations. After equilibration of 30 ns, CTAB micelle has an average total SASA of ~ 240 ± 4 nm^2 in water. The SASA values of CTAB micelle increased to ~ 256 ± 4 nm^2 and ~ 264 ± 4 nm^2 in 50 mM and 100 mM PG solution. The observed

changes in the total solvent-accessible area are contributed from the hydrophobic core of CTAB, which has a value of ~ 170 ± 3 nm^2 in water and increases to ~ 186 ± 4 nm^2 and ~ 194 ± 4 nm^2 in 50 mM and 100 mM PG solution respectively. The hydrophilic area remains around ~ 187 nm^2 in all the simulations. Simulation results depicted in Figure 8 (iv–vi) indicate that the major changes in micelle shapes and size are resulted from the changes in the hydrophobic core due to interactions of PG molecules with the CTAB hydrophilic area *i.e.*, the structural changes in the micellar aggregate are captured by MD study. It was observed that in 100 mM PG solution, the micellar aggregates show significant changes with more elongated hydrophobic chain and increased R_g values with enhanced hydrophobic core area. Thus, the simulation results support the experimental observation where CTAB micelle undergoes a successive micellar growth/transition as a function of [PG].

CONCLUSION

The self-associative behavior of CTAB in the presence of PG exhibited a synergistic effect where the CMC of CTAB was observed to decrease in the presence of [PG] depicting a profound efficiency of PG in reducing the surface tension of the investigated system. In addition, the oscillatory-shear outcomes of rheology indicated the viscoelastic behavior in the examined micellar solutions while the scattering findings gave a geometrical quantification expressed in terms of the intensity peak profile with distinct shifts in Q as a function of [PG] and temperature. The DFT analysis revealed small ΔE, and favorable interaction energies for the CTAB-PG system. Moreover, lower 3D-MEP showed a close proximity of CTAB with PG that emphasized favorable interaction between the nitrogen atom of CTAB and hydroxyl group of PG where 2D-NOESY complemented this findings and presented PG to be placed in the palisade layer through its alkyl chain-length near the micellar core. Especially, MD simulation offered an insight into the significant changes in micellar aggregates measured in terms of R_g and hydrophobic core area where the calculated R_g values inferred that the CTAB micelle stayed ellipsoidal throughout the simulation and that R_g values increased with [PG] in aqueous solution. In addition, the measured SASA offered an insight into the hydrophobic and hydrophilic properties of micellar system in aqueous solution where the SASA values of CTAB micelle increases during simulation which is contributed from the enhanced hydrophobic core of CTAB while the hydrophilic area remained constant in presence of PG. These simulation outcomes are unswerving with the scattering data that showed a significant effect of PG on the structure, dynamics, and aggregation properties of CTAB micelle. Thus, simulation and experimental results showed a good consistency, revealing a fine tuning in the self-assembly and interaction of stimulus-responsive surfactant-antioxidant systems depicting varied micellar morphology/architecture transition which can hold its plausible potential in surfactant-*based* formulations.

ACKNOWLEDGEMENT

V.K. acknowledges Department of Chemistry, Sardar Vallabhbhai National Institute of Technology (SVNIT), Gujarat for providing the instrumentation facility for analysis.

K.M.K. acknowledges support from National Science Foundation under Grant No. CHE-1665157, the Wichita State University Department of Chemistry and Fairmount College of Liberal Arts and Sciences; computational resources funded by the National Science Foundation under Award no. EPS-0903806 and matching support from the State of Kansas through the Kansas Board of Regents; and the National Institute of General Medical Sciences (P20

GM103418) from the National Institutes of Health. The content is solely the responsibility of the authors and does not necessarily represent the official views of the National Institute of General Medical Sciences or the National Institutes of Health.

REFERENCES

1. Schramm LL; Stasiuk EN; Marangoni DG, 2 Surfactants and their applications. Annual Reports Section" C"(Physical Chemistry) 2003, 99, 3–48.
2. Acharya DP; Kunieda H, Wormlike micelles in mixed surfactant solutions. Adv. Colloid Interface Sci 2006, 123, 401–413. [PubMed: 16860768]
3. Hyde A; Fujii S; Sakurai K; Phan C; Yusa S. i., Concentration-dependent Aggregation Behavior of Asymmetric Cationic Surfactant Hexyldimethyloctyl-ammonium Bromide. Chem. Lett 2017, 46, 271–273.
4. Kern F; Zana R; Candau S, Rheological properties of semidilute and concentrated aqueous solutions of cetyltrimethylammonium chloride in the presence of sodium salicylate and sodium chloride. Langmuir 1991, 7, 1344–1351.
5. Yin H; Lei S; Zhu S; Huang J; Ye J, Micelle-to-vesicle transition induced by organic additives in catanionic surfactant systems. Chem. Eur. J 2006, 12, 2825–2835. [PubMed: 16416498]
6. Davies TS; Ketner AM; Raghavan SR, Self-assembly of surfactant vesicles that transform into viscoelastic wormlike micelles upon heating. J. Am. Chem. Soc 2006, 128, 6669–6675. [PubMed: 16704268]
7. Kumar S; Aswal VK; Goyal PS, Effect of the addition of n-alkylamines on the growth of sodium decyl sulfate micelles. J. Chem. Soc. Faraday Trans 1996, 92, 2413–2415.
8. Patel V; Dharaiya N; Ray D; Aswal VK; Bahadur P, pH controlled size/shape in CTAB micelles with solubilized polar additives: a viscometry, scattering and spectral evaluation. Colloids Surf. A Physicochem. Eng. Asp 2014, 455, 67–75.
9. Krishnaswamy R; Ghosh SK; Lakshmanan S; Raghunathan V; Sood A, Phase behavior of concentrated aqueous solutions of cetyltrimethylammonium bromide (CTAB) and sodium hydroxy naphthoate (SHN). Langmuir 2005, 21, 10439–10443. [PubMed: 16262304]
10. Kuperkar K; Abezgauz L; Danino D; Verma G; Hassan P; Aswal V; Varade D; Bahadur P, Viscoelastic micellar water/CTAB/NaNO3 solutions: rheology, SANS and cryo-TEM analysis. J. Colloid Interf. Sci 2008, 323, 403–409.
11. Rodrigues RK; Da Silva MA; Sabadini E, Worm-like micelles of CTAB and sodium salicylate under turbulent flow. Langmuir 2008, 24, 13875–13879. [PubMed: 19053646]
12. Pal N; Kumar N; Mandal A, Stabilization of dispersed oil droplets in nanoemulsions by synergistic effects of Gemini surfactant, PHPA Polymer and Silica Nanoparticle. Langmuir 2019, 35, 2655–2667. [PubMed: 30672301]
13. Kumar GP; Rajeshwarrao P, Nonionic surfactant vesicular systems for effective drug delivery-an overview. Acta Pharm. Sin. B 2011, 1, 208–219.
14. Zhu X; Rohling R; Filonenko G; Mezari B; Hofmann JP; Asahina S; Hensen EJ, Synthesis of hierarchical zeolites using an inexpensive mono-quaternary ammonium surfactant as mesoporogen. Chem. commun 2014, 50, 14658–14661.
15. Wang X; Santo KP; Neimark AV, Modeling Gas-Interfaces by Dissipative Particle Dynamics: Adsorption and Surface Tension of Cetyl Trimethyl Ammonium Bromide at the Air-Water Interface. Langmuir 2020, 36, 14686–14698. [PubMed: 33216560]
16. Ge W; Kesselman E; Talmon Y; Hart DJ; Zakin JL, Effects of chemical structures of para-halobenzoates on micelle nanostructure, drag reduction and rheological behaviors of dilute CTAC solutions. J. Non-Newton. Fluid 2008, 154, 1–12.
17. Khatory A; Lequeux F; Kern F; Candau S, Linear and nonlinear viscoelasticity of semidilute solutions of wormlike micelles at high salt content. Langmuir 1993, 9, 1456–1464.
18. Kuperkar K; Abezgauz L; Prasad K; Bahadur P, Formation and growth of micelles in dilute aqueous CTAB solutions in the presence of $NaNO_3$ and $NaClO_3$. J. Surfactants Deterg 2010, 13, 293–303.

19. Aswal V; Goyal P; Thiyagarajan P, Small-angle neutron-scattering and viscosity studies of CTAB/NaSal viscoelastic micellar solutions. J. Phys. Chem. B 1998, 102, 2469–2473.
20. Agrawal NR; Yue X; Feng Y; Raghavan SR, Wormlike micelles of a cationic surfactant in polar organic solvents: Extending surfactant self-assembly to new systems and subzero temperatures. Langmuir 2019, 35, 12782–12791. [PubMed: 31525901]
21. Ito TH; Miranda PC; Morgon NH; Heerdt G; Dreiss C. c. A.; Sabadini E, Molecular variations in aromatic cosolutes: critical role in the rheology of cationic wormlike micelles. Langmuir 2014, 30, 11535–11542 [PubMed: 25222020]
22. Patel U; Dharaiya N; Bahadur P, Preservative solubilization induces microstructural change of Triton X-100 micelles. J. Mol. Liq 2016, 216, 156–163.
23. Boyce MC, Simultaneous determination of antioxidants, preservatives and sweeteners permitted as additives in food by mixed micellar electrokinetic chromatography. J. Chromatogr. A 1999, 847, 369–375. [PubMed: 10431367]
24. Heins A; Garamus VM; Steffen B; Stöckmann H; Schwarz K, Impact of phenolic antioxidants on structural properties of micellar solutions. Food Biophys 2006, 1, 189–201.
25. Zaccheroni N; Amorati R; Mezzina E; Baschieri A; Palomba F; Prata C; Facchini C; Guernelli S, Antioxidant effect of cardanol in mixed nanoformulations with pluronic. J. Mol. Liq 2020, 316, 113822.
26. Andrzejewska A; Narkiewicz-Michalek J; Szymula M, Co-Adsorption of CTAB and Propyl Gallate on the Hydrophilic Silica Surface. J. Dispers. Sci. Technol 2007, 28 (2), 239–245.
27. Heins A; McPhail DB; Sokolowski T; Stöckmann H; Schwarz K, The location of phenolic antioxidants and radicals at interfaces determines their activity. Lipids 2007, 42, 573–582. [PubMed: 17473943]
28. Szymula M; Narkiewicz-Michałek J, The effect of surfactant adsorption at a glassy carbon electrode on electrochemical oxidation of propyl gallate. J. Appl. Electrochem 2006, 36 (4), 455–462.
29. Piotrovskaya E; Vanin A; Smirnova N, Molecular dynamics simulation of micellar aggregates in aqueous solution of hexadecyl trimethylammonium chloride with different additives. Mol. Phys 2006, 104, 3645–3651.
30. Shelley JC; Shelley MY, Computer simulation of surfactant solutions. Curr. Opin. Colloid Interface Sci 2000, 5, 101–110.
31. Rajagopalan R, Simulations of self-assembling systems. Curr. Opin. Colloid Interface Sci 2001, 6, 357–365.
32. Verma R; Mishra A; Mitchell-Koch KR, Molecular modeling of cetylpyridinium bromide, a cationic surfactant, in solutions and micelle. J. Chem. Theory Comput 2015, 11, 5415–5425. [PubMed: 26574330]
33. Sangwai AV; Sureshkumar R, Coarse-grained molecular dynamics simulations of the sphere to rod transition in surfactant micelles. Langmuir 2011, 27, 6628–6638. [PubMed: 21524093]
34. Yuan S; Ma L; Zhang X; Zheng L, Molecular dynamics studies on monolayer of cetyltrimethylammonium bromide surfactant formed at the air/water interface. Colloids Surf. A Physicochem. Eng. Asp 2006, 289, 1–9.
35. Velinova M; Sengupta D; Tadjer AV; Marrink S-J, Sphere-to-rod transitions of nonionic surfactant micelles in aqueous solution modeled by molecular dynamics simulations. Langmuir 2011, 27, 14071–14077. [PubMed: 21981373]
36. Chen J; Hao J, Molecular dynamics simulation of cetyltrimethylammonium bromide and sodium octyl sulfate mixtures: aggregate shape and local surfactant distribution. Phys. Chem. Chem. Phys 2013, 15, 5563–5571. [PubMed: 23463240]
37. Kumar V; Patel D; Pal H; Kuperkar K, A comprehensive insight on H-type aggregation in Congo red-surfactant systems revealed through spectroscopic and electrochemical study unified with a simulation framework. Phys. Chem. Chem. Phys 2019, 21, 15584–15594. [PubMed: 31268439]
38. Kuperkar K; Modi J; Patel K, Surface-active properties and antimicrobial study of conventional cationic and synthesized symmetrical gemini surfactants. J. Surfactants Deterg 2012, 15, 107–115.
39. Czajka A; Hazell G; Eastoe J, Surfactants at the design limit. Langmuir 2015, 31, 8205–8217. [PubMed: 25797065]

40. Aswal V; Goyal P, Small-angle neutron scattering diffractometer at Dhruva reactor. Curr. Sci 2000, 79, 947–953.
41. Patel D; Ray D; Kuperkar K; Aswal VK; Bahadur P, Parabens induced spherical micelle to polymersome transition in thermo-responsive amphiphilic linear and star-shaped EO-PO block copolymers. J. Mol. Liq 2020, 316, 113897.
42. Soni SS; Sastry NV; Aswal VK; Goyal PS, Micellar structure of silicone surfactants in water from surface activity, SANS and viscosity studies. J. Phys. Chem. B 2002, 106, 2606–2617.
43. Kuperkar K; Patriati A; Putra E; Singh K; Marangoni D; Bahadur P, Microstructural study of cetyltrimethylammonium bromide/1-butanol/salt/water system-SANS and 2D-NOESY analysis. Can. J. Chem 2012, 90, 314–320.
44. Chavda S; Singh K; Gerrard Marangoni D; Aswal VK; Bahadur P, Cationic Micelles Modulated in the Presence of α, ω-Alkanediols: A SANS, NMR and Conductometric Study. J. Surfactants Deterg 2012, 15 (3), 317–325.
45. Yuan H; Luo L; Zhang L; Zhao S; Mao S; Yu J; Shen L; Du Y, Aggregation of sodium dodecyl sulfate in poly (ethylene glycol) aqueous solution studied by ^{1}H-NMR spectroscopy. Colloid Polym. Sci 2002, 280, 479–484.
46. Kanoje B; Jangir A; Patel D; Ray D; Aswal V; Pal H; Parikh J; Kuperkar K, Micellar transition (ellipsoidal to ULV) induced in aqueous Gemini surfactant (12-2-12) solution as a function of additive concentration and temperature using experimental and theoretical study. Colloids Surf. A Physicochem. Eng. Asp 2018, 555, 227–236.
47. Jangir AK; Lad B; Dani U; Shah N; Kuperkar K, In vitro toxicity assessment and enhanced drug solubility profile of green deep eutectic solvent derivatives (DESDs) combined with theoretical validation. RSC Adv 2020, 10, 24063–24072.
48. Abraham MJ; Murtola T; Schulz R; Páll S; Smith JC; Hess B; Lindahl E, GROMACS: High performance molecular simulations through multi-level parallelism from laptops to supercomputers. SoftwareX 2015, 1–2, 19–25.
49. Martínez JM; Martínez L, Packing optimization for automated generation of complex system's initial configurations for molecular dynamics and docking. J. Comput. Chem 2003, 24, 819–825. [PubMed: 12692791]
50. Schmid N; Eichenberger AP; Choutko A; Riniker S; Winger M; Mark AE; van Gunsteren WF, Definition and testing of the GROMOS force-field versions 54A7 and 54B7. Eur. Biophys. J 2011, 40, 843. [PubMed: 21533652]
51. Malde AK; Zuo L; Breeze M; Stroet M; Poger D; Nair PC; Oostenbrink C; Mark AE, An Automated Force Field Topology Builder (ATB) and Repository: Version 1.0. J. Chem. Theory Comput 2011, 7, 4026–4037. [PubMed: 26598349]
52. Stroet M; Caron B; Visscher KM; Geerke DP; Malde AK; Mark AE, Automated Topology Builder Version 3.0: Prediction of Solvation Free Enthalpies in Water and Hexane. J. Chem. Theory Comput 2018, 14, 5834–5845. [PubMed: 30289710]
53. Kumar V; Pal N; Jangir AK; Manyala DL; Varade D; Mandal A; Kuperkar K, Dynamic interfacial properties and tuning aqueous foamability stabilized by cationic surfactants in terms of their structural hydrophobicity, free drainage and bubble extent. Colloids Surf. A Physicochem. Eng. Asp 2020, 588, 124362.
54. del Mar Graciani M; Rodríguez A; Muñoz M; Moyá ML, Micellar Solutions of Sulfobetaine Surfactants in Water-Ethylene Glycol Mixtures: Surface tension, fluorescence, spectroscopic, conductometric, and kinetic studies. Langmuir 2005, 21, 7161–7169. [PubMed: 16042437]
55. Li R; Zhang Q; Pei X; Xie D; Song B, The rheological behavior of organic salt/Gemini surfactant mixed systems: Effect of isomerization of additives. Colloids Surf. A Physicochem. Eng. Asp 2020, 585, 124114.
56. Yan Z; Dai C; Zhao M; Sun Y, Rheological characterizations and molecular dynamics simulations of self-assembly in an anionic/cationic surfactant mixture. Soft matter 2016, 12, 6058–6066. [PubMed: 27373717]
57. Raghavan SR; Kaler EW, Highly viscoelastic wormlike micellar solutions formed by cationic surfactants with long unsaturated tails. Langmuir 2001, 17, 300–306.
58. Chuab Z; Feng Y, Thermo-switchable surfactant gelw. Chem. Commun 2011, 47, 7191–7193.

59. Padsala S; Dharaiya N; Sastry NV; Aswal VK; Bahadur P, Microstructural morphologies of CTAB micelles modulated by aromatic acids. RSC adv 2016, 6, 105035–105045.

60. Shrestha RG; Sakai K; Sakai H; Abe M, Rheological properties of polyoxyethylene cholesteryl ether wormlike micelles in aqueous system. J. Phys. Chem. B 2011, 115, 2937–2946. [PubMed: 21370836]

61. Aswal V; Goyal P, Role of counterion distribution on the structure of micelles in aqueous salt solutions: small-angle neutron scattering study. Chem. Phys. Lett 2002, 357, 491–497.

62. Dharaiya N; Chavda S; Singh K; Marangoni D; Bahadur P, Spectral and hydrodynamic studies on p-toluidine induced growth in cationic micelle. Spectrochim. Acta A 2012, 93, 306–312.

63. Heins A; Sokolowski T; Stöckmann H; Schwarz K, Investigating the location of propyl gallate at surfaces and its chemical microenvironment by ^{1}H-NMR. Lipids 2007, 42, 561–572. [PubMed: 17447096]

64. Patel D; Ray D; Kuperkar K; Pal H; Aswal VK; Bahadur P, Solubilization, micellar transition and biocidal assay of loaded antioxidants in Tetronic® 1304 micelles. Polym. Int 2020. 10.1002/pi.5962

65. Patel D; Rathod S; Tiwari S; Ray D; Kuperkar K; Aswal VK; Bahadur P, Self-Association in EO-BO-EO Triblock Copolymers as a Nanocarrier Template for Sustainable Release of Anticancer Drugs. J. Phys. Chem. B 2020, 124, 11750–11761. [PubMed: 33305575]

66. Catá GF; Rojas HC; Gramatges AP; Zicovich-Wilson CM; Álvarez LJ; Searle C, Initial structure of cetyltrimethylammonium bromide micelles in aqueous solution from molecular dynamics simulations. Soft Matter 2011, 7, 8508–8515.

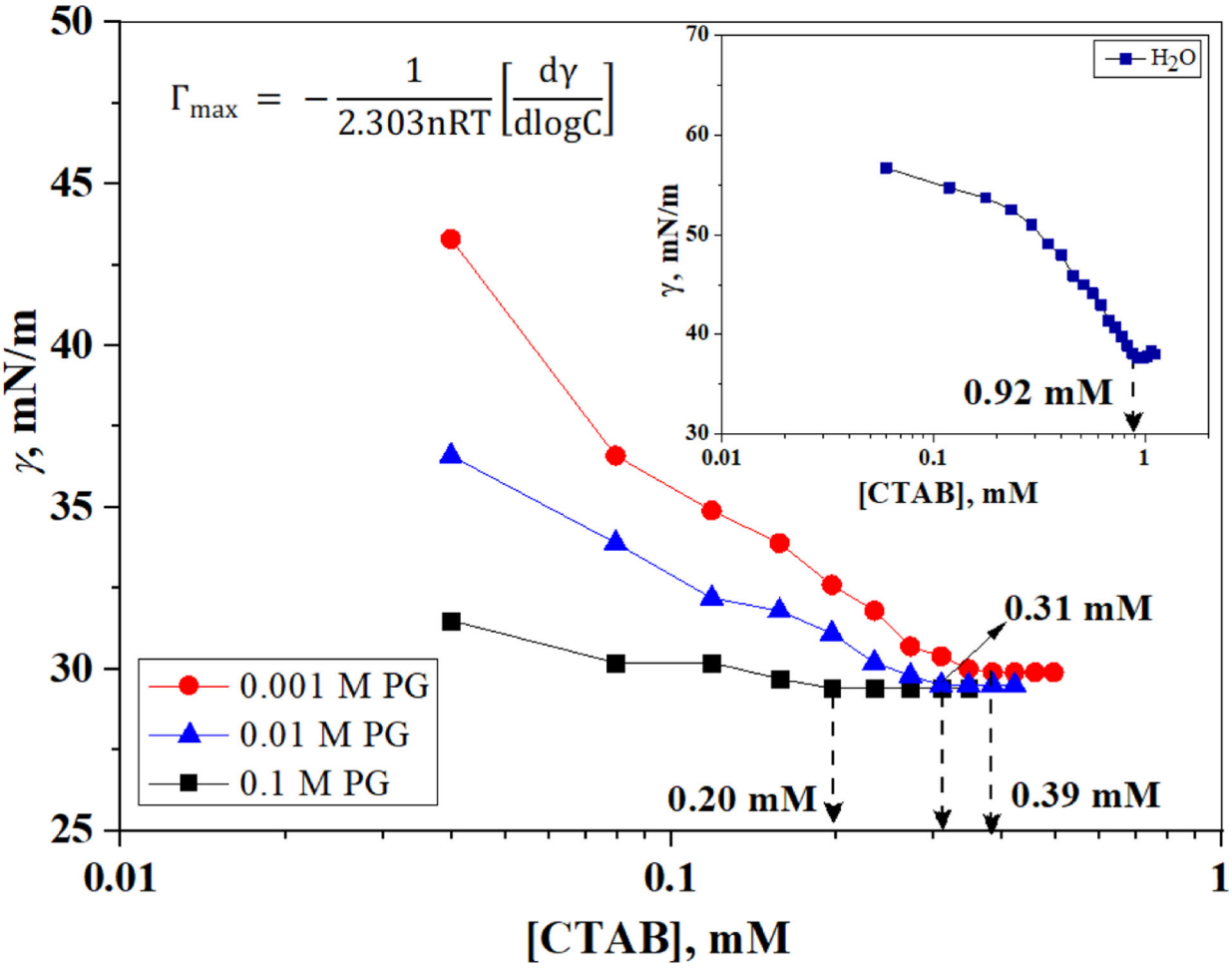

Figure 1.
Surface tension (ST, γ) plot of CTAB in the presence of varying [PG] at 30 °C.

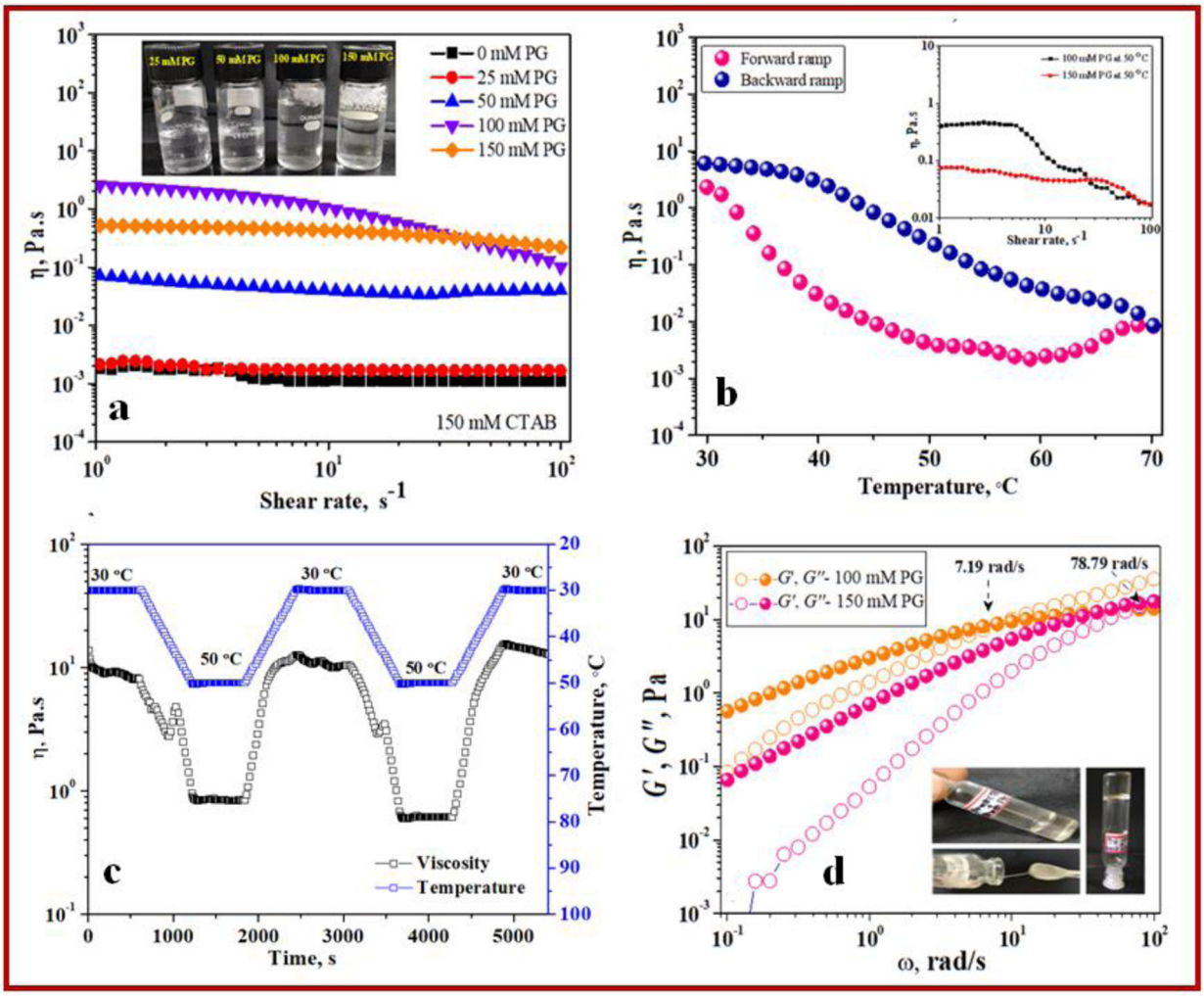

Figure 2.

Viscosity (η) trend in 150 mM CTAB solution at varying [PG] as a function of: (a) shear rate at 30 °C and (b) temperature. (c) The thermo-reversible rheological response of the 150 mM CTAB in presence of 150 mM PG. The temperature was controlled via a preset procedure and the resulting apparent viscosity was measured at a shear rate of 1 s^{-1}, and (d) The dynamic viscoelastic behavior depicting the dependence of ω for 150 mM CTAB at varying [PG] at 30 °C. *Snapshots of the vials in the Figure indicate the physical appearance of the solution behavior for the examined system.*

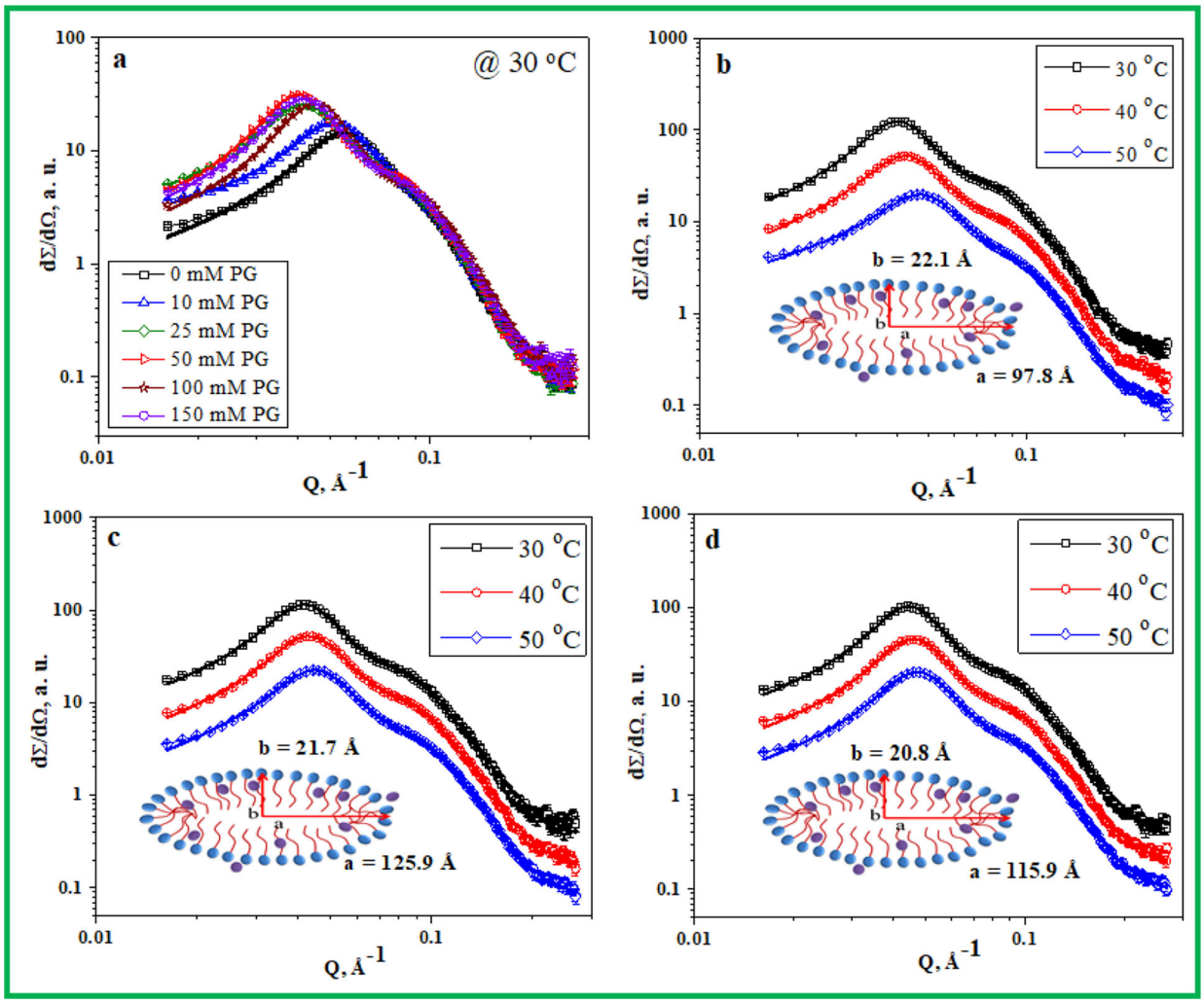

Figure 3.

Scattering profile for 150 mM CTAB (a) in varying [PG] at 30 °C and in presence of (b) 50 mM, (c) 100 mM PG, and (d) 150 mM PG at different temperatures. *(The solid lines represent the best fit with model used for ellipsoidal micellar morphology).* The spectral profile presented in Figure 3b, 3c and 3d has been shifted vertically by multiplying a factor of *2* for clarity of the presentation.

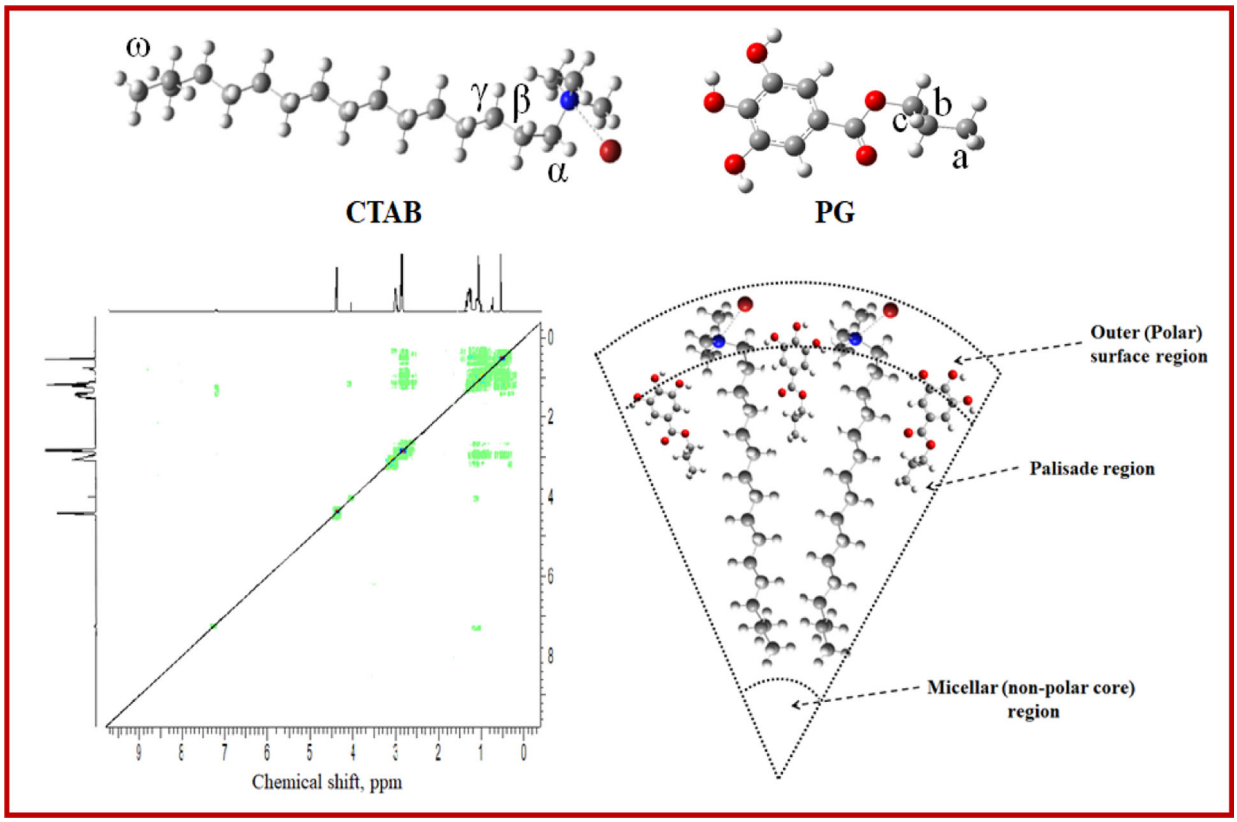

Figure 4.

Optimized structure of CTAB and PG with labelling assigned to their respective protons undergoing the plausible interactions as depicted by 2D-NOESY along with the schematic representation.

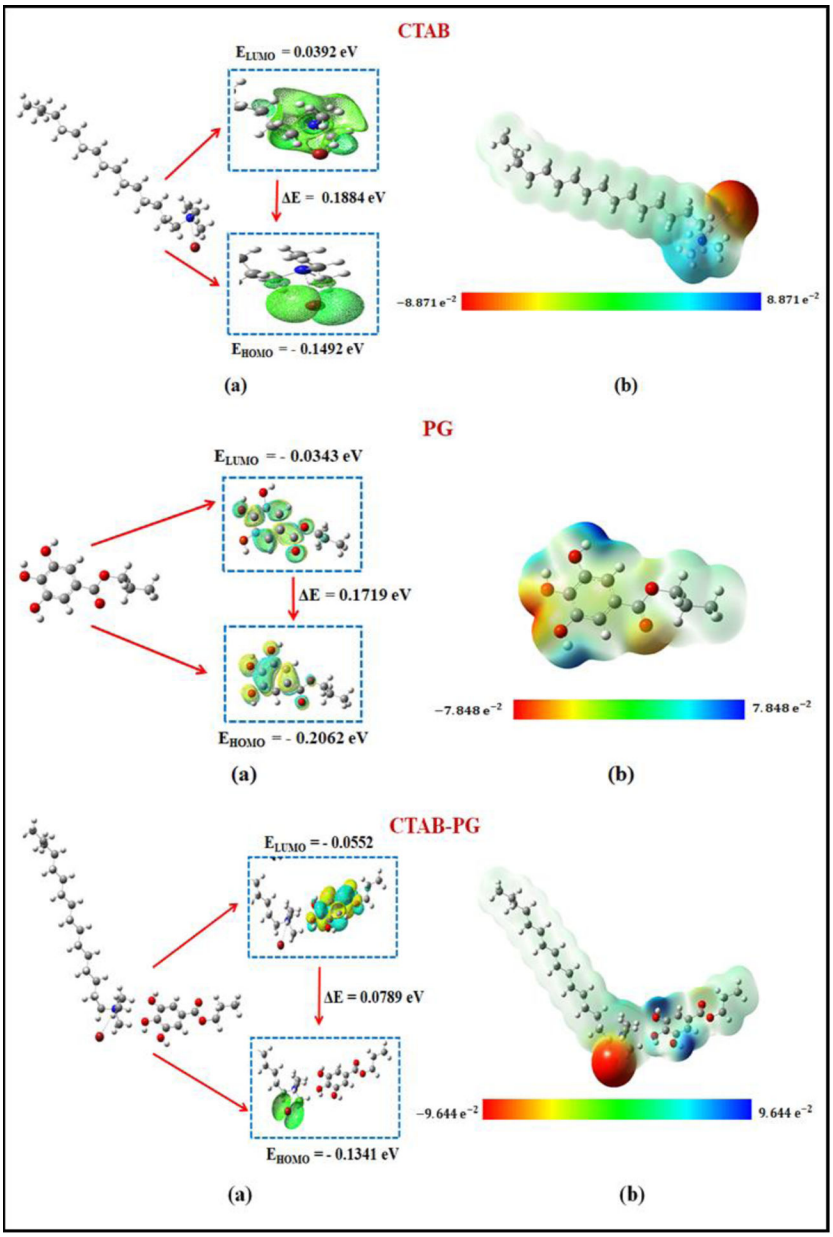

Figure 5.

(a) The optimized HOMO-LUMO lobes depicting the ΔE (in eV) and (b) Color 3D-surface molecular electrostatic potential (ESP) in CTAB, PG and CTAB-PG system.

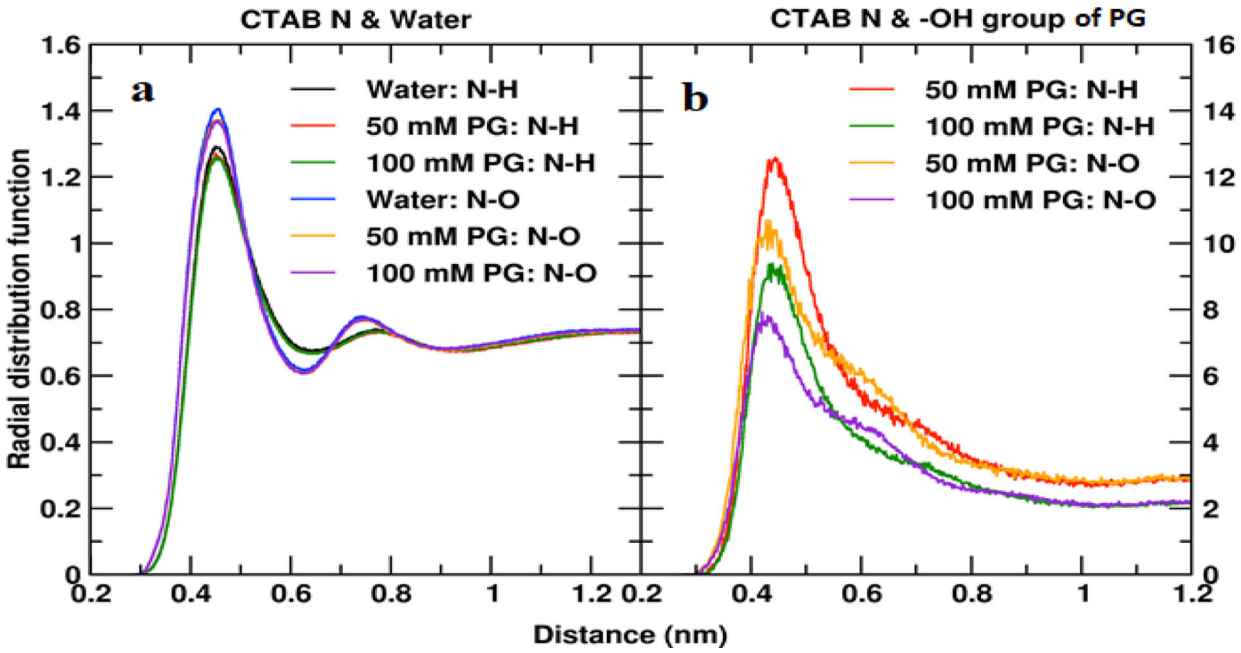

Figure 6.

The radial distribution function (RDF) for the solvent atoms is shown from the N atom of CTAB monomer for H and O of (a) water molecules, and (b) PG −OH group around CTAB micelle.

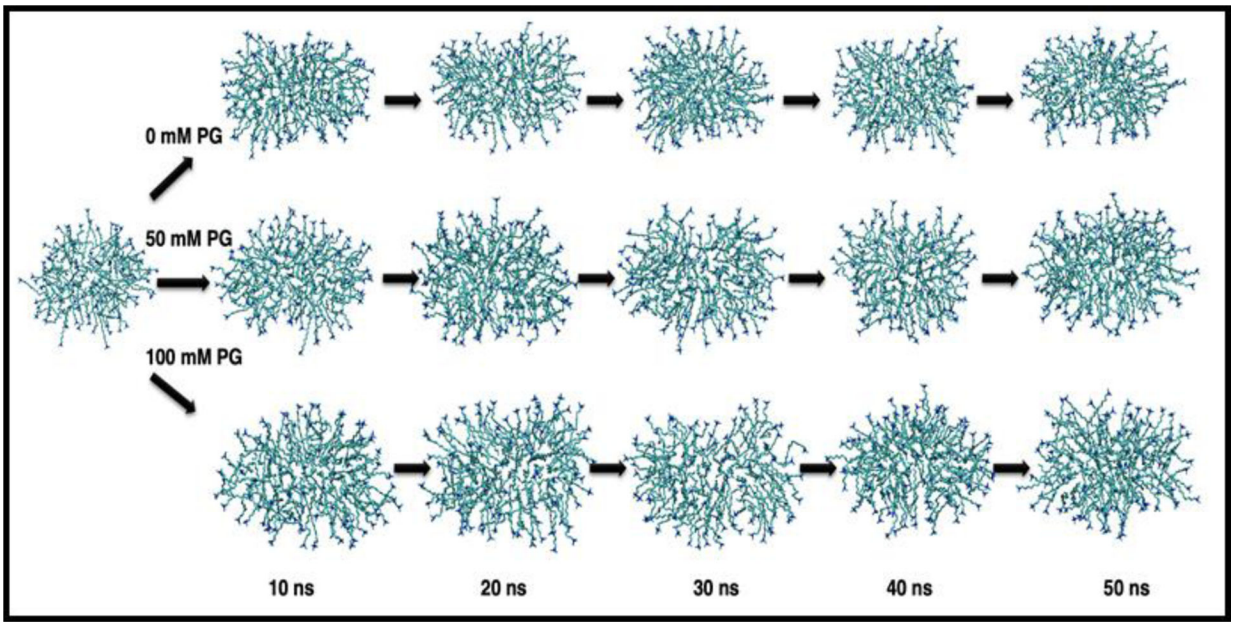

Figure 7.

Snapshots of CTAB micelle in the aqueous solution environment comprising of 0 mM, 50 mM, and 100 mM PG starting from an equilibrated structure (0 ns) followed by every 10 ns intervals up to 50 ns. (*The arrow shows the progression of the simulation, with labelled simulation time in ns aggregates thereby giving a hint on their shape and dynamics*). Here, the simulation data show a profound effect of the phenolic −OH group on the micelle morphology.

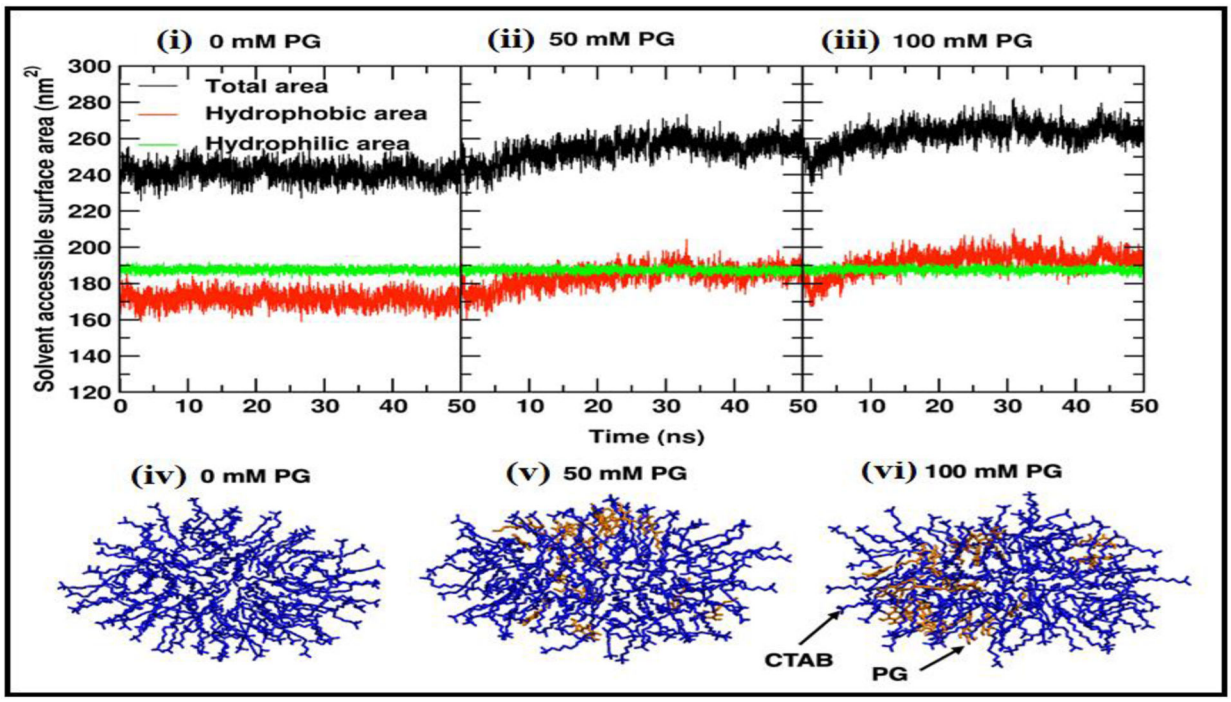

Figure 8.

The solvent accessible surface area (SASA) of CTAB micelle as a function of time is shown in (i) water, and (ii) 50 mM PG and (iii) 100 mM PG. The 150 mM CTAB micelle from the last frame of 50 ns simulation in presence of (iv) 0 mM PG (v) 50 mM and (vi) 100 mM PG are shown in licorice representation.

Table 1:

Simulation details of CTAB micelles in solution.

System	CTAB Monomers/Br^- Ions	PG concentration (mM)	PG Molecules	Water Molecules	Total Number of Atoms
1	100	0	0	37064	113292
2	100	50	33	36621	112623
3	100	100	66	36304	112332

Table 2.

Interfacial parameters of CTAB as a function of [PG] at 30 °C.

[PG], mM	CMC (mM)	γ_{CMC} (mN/m)	Γ_{max} ($x10^{-6}$ mol m^{-2})	π_{CMC} (mN/m)
0.0	0.92	37.6	2.47	32.6
0.001	0.39	29.8	0.99	40.4
0.01	0.31	29.5	0.61	40.7
0.1	0.20	29.4	0.19	40.8

Table 3.

SANS parameters evaluated for 150 mM CTAB micelles inferring the ellipsoidal geometry as a function of [PG] and temperature.

150 mM CTAB + [PG]	T (°C)	Semi-major axis *a* (Å)	Semi-minor axis *b* (Å)	Axial ratio *a*/*b*	Hard sphere radius R_{hs} (Å)	Volume fraction Φ	Fractional charge α (esu)	Aggregation number N_{agg}
0 mM	30	35.6	22.8	1.6	51.8	0.26	0.18	138
10 mM	30	41.6	22.5	1.9	56.6	0.25	0.09	158
25 mM	30	90.2	21.9	4.1	66.9	0.23	0.11	324
50 mM	30	97.8	22.1	4.4	70.5	0.28	0.13	357
	40	86.0	21.7	4.0	65.8	0.28	0.13	303
	50	64.6	21.1	3.1	59.5	0.31	0.11	215
100 mM	30	125.9	21.7	5.8	67.7	0.28	0.11	443
	40	114.4	21.3	5.4	64.7	0.28	0.12	388
	50	94.6	20.7	4.6	62.1	0.29	0.14	303
150 mM	30	115.9	20.8	5.6	63.4	0.27	0.13	375
	40	105.4	20.7	5.1	61.5	0.28	0.14	338
	50	97.8	20.3	4.8	59.1	0.28	0.15	301